OPEN ACCESS Freely available online

PLoS GENETICS

Mutations in Zebrafish *lrp2* Result in Adult-Onset Ocular Pathogenesis That Models Myopia and Other Risk Factors for Glaucoma

Kerry N. Veth[1], Jason R. Willer[2], Ross F. Collery[1], Matthew P. Gray[1], Gregory B. Willer[2], Daniel S. Wagner[3], Mary C. Mullins[4], Ava J. Udvadia[5], Richard S. Smith[6], Simon W. M. John[6], Ronald G. Gregg[2], Brian A. Link[1]*

1 Department of Cell Biology, Neurobiology, and Anatomy, Medical College of Wisconsin, Milwaukee, Wisconsin, United States of America, **2** Department of Biochemistry and Molecular Biology, University of Louisville, Louisville, Kentucky, United States of America, **3** Department of Biochemistry and Cell Biology, Rice University, Houston, Texas, United States of America, **4** Department of Cell and Developmental Biology, University of Pennsylvania Medical School, Philadelphia, Pennsylvania, United States of America, **5** Department of Biological Sciences, University of Wisconsin–Milwaukee, Milwaukee, Wisconsin, United States of America, **6** Howard Hughes Medical Institute, The Jackson Laboratory, Bar Harbor, Maine, United States of America

Abstract

The glaucomas comprise a genetically complex group of retinal neuropathies that typically occur late in life and are characterized by progressive pathology of the optic nerve head and degeneration of retinal ganglion cells. In addition to age and family history, other significant risk factors for glaucoma include elevated intraocular pressure (IOP) and myopia. The complexity of glaucoma has made it difficult to model in animals, but also challenging to identify responsible genes. We have used zebrafish to identify a genetically complex, recessive mutant that shows risk factors for glaucoma including adult onset severe myopia, elevated IOP, and progressive retinal ganglion cell pathology. Positional cloning and analysis of a non-complementing allele indicated that non-sense mutations in *low density lipoprotein receptor-related protein 2* (*lrp2*) underlie the mutant phenotype. Lrp2, previously named Megalin, functions as an endocytic receptor for a wide-variety of bioactive molecules including Sonic hedgehog, Bone morphogenic protein 4, retinol-binding protein, vitamin D-binding protein, and apolipoprotein E, among others. Detailed phenotype analyses indicated that as *lrp2* mutant fish age, many individuals—but not all—develop high IOP and severe myopia with obviously enlarged eye globes. This results in retinal stretch and prolonged stress to retinal ganglion cells, which ultimately show signs of pathogenesis. Our studies implicate altered Lrp2-mediated homeostasis as important for myopia and other risk factors for glaucoma in humans and establish a new genetic model for further study of phenotypes associated with this disease.

Citation: Veth KN, Willer JR, Collery RF, Gray MP, Willer GB, et al. (2011) Mutations in Zebrafish *lrp2* Result in Adult-Onset Ocular Pathogenesis That Models Myopia and Other Risk Factors for Glaucoma. PLoS Genet 7(2): e1001310. doi:10.1371/journal.pgen.1001310

Editor: Janey Wiggs, Harvard University, United States of America

Received September 24, 2010; **Accepted** January 13, 2011; **Published** February 17, 2011

Funding: This work was supported by National Institutes of Heath (NIH) grant R01EY016060 (BAL). SWMJ is an Investigator of the Howard Hughes Medical Institute. The funders had no role in study design, data collection and analysis, decision to publish, or preparation of the manuscript.

Competing Interests: The authors have declared that no competing interests exist.

* E-mail: blink@mcw.edu

Introduction

The multi-factorial nature of many ocular diseases poses a major challenge in understanding their molecular etiology and in engineering animal models to study mechanisms of pathology. Macular degeneration, myopia, and glaucoma are examples of prevalent and disruptive complex ocular diseases. While characterization of complement factor genes has provided insight into most cases of macular degeneration [1], no major genetic pathway has been found to underlie myopia or glaucoma. Myopia is the most common human ocular disorder worldwide and is caused by abnormal growth of the eye resulting in refractive error [2,3]. Myopia also increases risk for other visual impairing diseases including glaucoma [4]. The glaucomas are a heterogeneous group of progressive blinding disorders that result from damage to retinal ganglion cells and their axons [5]. Important risk factors for glaucoma include elevated intraocular pressure (IOP), age, family history, and myopia [6]. Although traditional human genetic analysis has been limited in identifying causative genes for complex disorders, mutational screens in animals can provide insights into disease etiology. Recently, progress has been made on establishing the zebrafish model to study phenotypes associated with glaucoma. From a forward-genetic perspective, zebrafish offer a major advantage in studying complex disease, in that large pedigrees can be efficiently generated with moderate space and time requirements.

Through a mutational screen for adult ocular defects, we identified a complex mutant, *bugeye*, that manifests multiple adult-onset phenotypes associated with glaucoma including enlarged eyes with myopia, elevated IOP, and damage to retinal ganglion cells. Using linkage analysis we discovered non-sense mutations in *low density lipoprotein receptor-related protein 2* (*lrp2*) for *bugeye*, as well as within a non-complementing allele. Lrp2 is a large transmembrane protein of the LDL-receptor related protein (Lrp) family [7]. Lrp2 participates in receptor-mediated endocytosis and has a host of identified ligands including signaling molecules like Sonic

Author Summary

Complex genetic inheritance, including variable penetrance and severity, underlies many common eye diseases. In this study, we present analysis of a zebrafish mutant, *bugeye*, which shows complex inheritance of multiple ocular phenotypes that are known risk factors for glaucoma, including high myopia, elevated intraocular pressure, and up-regulation of stress-response genes in retinal ganglion cells. Molecular genetic analysis revealed that mutations in *low density lipoprotein receptor-related protein 2 (lrp2)* underlie the mutant phenotypes. Lrp2 is a large transmembrane protein expressed in epithelia of the eye. It facilitates transport and clearance of multiple secreted bioactive factors through receptor-mediated endocytosis. Glaucoma, a progressive blinding disorder, usually presents in adulthood and is characterized by optic nerve damage followed by ganglion cell death. In *bugeye/lrp2* mutants, ganglion cell death was significantly elevated, but surprisingly moderate, and therefore they do not model this endpoint of glaucoma. As such, *bugeye/lrp2* mutants should be considered valuable as a genetic model (A) for buphthalmia, myopia, and regulated eye growth; (B) for identifying genes and pathways that modify the observed ocular phenotypes; and (C) for studying the initiation of retinal ganglion cell pathology in the context of high myopia and elevated intraocular pressure.

hedgehog and Bone morphogenetic protein 4, vitamin and hormone binding proteins, apolipoproteins, among others [8]. Lrp2 is expressed on cells of the renal proximal tubule, choroid plexus, developing neural tube, intestine, thyroid, and inner ear. Within the eye, Lrp2 is expressed on retinal pigment epithelial cells as well as ciliary epithelial cells [7–9]. In humans, mutations in *LRP2* result in Donnai-Barrow syndrome [10], a rare disease characterized by a spectrum of phenotypes including agenesis of the corpus collosum, diaphragmatic hernia, sensonurial deafness, hypertelorism, buphthalmia (enlarged eye globes) and high myopia [11,12]. As the eyes of *bugeye* zebrafish are also highly myopic, Lrp2 may be critical in regulating emmetropic eye growth across species. The strong association of myopia with glaucoma [13] makes *bugeye* an attractive model to study the genetic and molecular pathways involved in these ocular diseases.

Results

Identification of an enlarged eye mutant with elevated intraocular pressure

The *bugeye* zebrafish mutant was identified in a three-generation forward-genetic screen for adult ocular abnormalities. Mutants were easily identified by 6 months as their eyes were visibly enlarged (Figure 1A, 1C). Interestingly, the degree of eye enlargement often varied between the two eyes of a single fish (Figure S1A–S1G). Occasionally the phenotype presented only in one eye, and the other eye remained normal in size (Figure S1B). To address whether ocular enlargement in mutants might represent a retinoblastoma phenotype, we analyzed eyes by histology. Instead of obvious cellular overgrowth we found that the retina was notably thinner in all layers (Figure 1B, 1D). As buphthalmia is often associated with elevated IOP, we used servo-null electrophysiology to measure the eye pressures in mutants and wild-type siblings [14]. Compared to wild-type fish, *bugeye* mutants consistently showed elevated IOPs (Figure 1I). In addition, the rare fish that presented the phenotype in a unilateral manner had normal pressure in the wild-type sized eye and elevated pressure in the enlarged eye (Figure S1H). IOP is maintained by the balance of aqueous humor production and drainage. Like mammals, aqueous humor in zebrafish is produced in the ciliary epithelium and drained at the iridocorneal angle. However, unlike mammals where drainage occurs circumferentially throughout the angle region, aqueous outflow for zebrafish is facilitated through a discrete ventrally localized canalicular network [15]. Histology did not reveal obvious disorganization in either the dorsal ciliary epithelium (Figure 1E, 1G) or in the ventral canalicular outflow network (Figure 1F, 1H). However, the ciliary epithelium occasionally appeared mildly hypertrophied (Figure 1G, arrow) and the angle region of mutants was more prone than wild-type specimens to separation between the iris and corneal tissues during histological preparation (Figure 1H, asterisk). Additional characterization of these regions at the time of phenotype onset confirmed these observations (Figure S2).

Mutations in *lrp2* underlie the complex *bugeye* phenotype

The original *bugeye* mutants presented in the third generation of a three-generation screen, suggesting the mutation was recessive. However, only 3 fish out of a family of 28 showed the phenotype and therefore the penetrance was lower than predicted for a

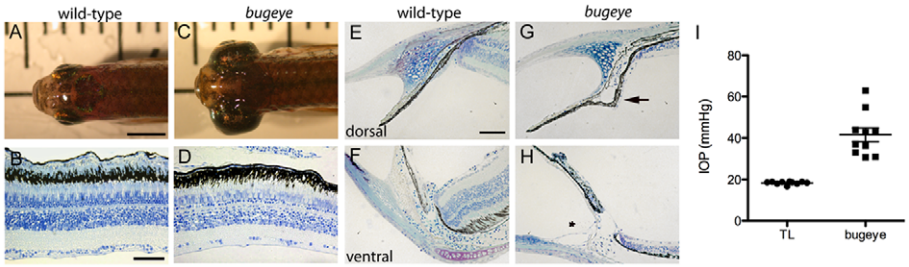

Figure 1. Adult *bugeye* zebrafish have enlarged eye globes, thinned retinas, and elevated intraocular pressure without iridocorneal angle obstruction or malformation. *A,C* Dorsal views of adult wild-type (A) and *bugeye* (C) zebrafish. *B,D* Histology of central retina sections at 6 months in wild-type (B) and mutant (D) eyes. *E-H* Histology of wild-type (E,F) and *bugeye* mutant (G,H) iridocorneal angles in the dorsal region (E,G) or at the ventral canalicular aqueous humor drainage region (F,H). *I* Intraocular pressures (IOP) in adult wild-type and *bugeye* zebrafish. IOPs in *bugeye* fish were elevated compared to age and size matched fish from TL wild-type stain ($p<0.0001$, t-test). Scale bars: A,C = 4 mm; B,D = 50 μm; E-H = 40 μm.
doi:10.1371/journal.pgen.1001310.g001

simple recessive mutation (~9% vs. 25% predicted). Moreover, incrossing 2 of those original mutant fish resulted in 25 progeny that showed large eyes and 18 that never developed the phenotype. Again, if the mutation was a simple recessive mutation, incrossing should have resulted in all progeny showing the phenotype. To better characterize inheritance and establish recombinant mapping panels to genetically position the mutant locus, we set up a series of test-crosses. Table 1 summarizes the results of incross, outcross and backcross matings over multiple generations and genetic backgrounds (Table 1). The data indicate that the *bugeye* phenotype is most likely caused by a single recessive mutation, but like many multi-factorial complex diseases, the penetrance was modified by common wild-type backgrounds and/or by non-genetic factors.

To map the mutant locus, progeny from single pair backcross matings were used for whole-genome linkage analysis. Co-segregation for markers on chromosome 9 and the mutant phenotype was found (Figure 2A). Informatively, no other linkage in the genome was noted, consistent with the single recessive causative mutation hypothesis. Public databases revealed that the *lrp2* gene was within the critical recombinant interval. Given the similarity of the *bugeye* phenotype to those caused by *LRP2* mutations in humans, we sequenced this candidate gene. Analysis of *lrp2* cDNA from *bugeye*^{mw1} mutants revealed a T to A conversion that changes a cysteine to a stop codon at predicted amino acid position 23 (C23X) (Figure 2B, 2C). Through an independent genetic screen we identified a second large eye mutant that like the *bugeye*^{mw1} allele, presented in adulthood and showed reduced penetrance. Intercrosses between this mutant (allele p5bnc) and *bugeye*^{mw1} were non-complementing and suggested that *lrp2* may also be affected in the p5bnc mutant. Indeed, sequencing of p5bnc cDNA revealed a separate non-sense mutation, also very early in the coding region of *lrp2* (*bugeye*^{p5bnc}, Q413X) (Figure 2B, 2C). To test whether somatic reversion or alternate splicing around the non-sense mutations might underlie the reduced penetrance or variability often observed between the left and right eyes, we sequenced ocular cDNA in affected and unaffected eyes. However, we did not find evidence of mosaicism or alternate splicing surrounding the mutations, suggesting the penetrance and phenotype variability is influenced by other genes, epigenetics, and/or unpredictable changes in physiology which affects the phenotypes.

In mammalian eyes, the multi-ligand receptor Lrp2 is known to be expressed in the developing and adult retinal pigment epithelium (RPE) and ciliary epithelium. We therefore analyzed Lrp2 expression in wild-type, *bugeye* mutant larvae treated with phenyl-thio-urea (PTU), which blocks pigmentation and allows visualization of potential RPE immunoreactivity. As predicted, strong immunoreactivity was found in wild-type RPE and ciliary epithelium. Other regions of expression noted in wild-type fish included forebrain ventricles, regions of the inner ear, proximal pronephros, and gut epithelium (data not shown). All Lrp2 immunoreactivity was completely absent in mutant larvae for both *bugeye* alleles (Figure 2D, 2E and data not shown). We next developed genotyping protocols for both mutant alleles and confirmed that large-eyed fish never showed wild-type *lrp2* genotypes (Figure 2F, 2G). We also used this assay to test whether the reduced penetrance of the ocular phenotype could be explained by increased larval lethality of *lrp2* mutants. However, we found that all genotypes were represented in Mendelian ratios in the adult progeny of either heterozygous or backcross pairwise matings, despite the fact that some homozygous mutants never developed the enlarged eye phenotype. Cumulatively, these data indicate that *lrp2* mutations are responsible for the large-eyed phenotype in *bugeye* and that the reduced penetrance and variability in eye enlargement are due to either common (yet unknown) genetic background differences and/or non-genetic factors such as physiological modifiers of the mutation.

Lrp2 mutants show adult onset buphthalmia and progressive myopia

Having established the causative gene for *bugeye*, we next investigated the onset of the ocular phenotype and quantified the pathology. To characterize the development of enlarged eyes in *bugeye/lrp2* mutants we performed longitudinal studies tracking wild-type and mutant fish from 1-12 months. The zebrafish eye reaches its final adult anatomy by approximately 1 month of age [16]. Because overall growth rates can vary between equally aged fish — even within the same tank — we used the ratio of eye size to body length (E:B) to determine the relative size of the eye. This ratio remained constant in wild-type fish, allowing comparison of relative eye size between individuals regardless of the overall growth of the fish. Although this ratio remained flat as wild-type fish grew, the E:B ratio increased over time for most

Table 1. Inheritance and penetrance of large eye phenotype.

Mutation	Type of test cross	Progeny Analyzed (*n*)	Large eye Phenotype (%)	Expected for Recessive (%)
lrp2 C23X	Incross [a]	528	66 [d]	100
(*bug*^{mw1})	Outcross [b]	856	0	0
	Backcross [c]	2094	11	50
lrp2 Q413X	Incross [a]	213	87 [d]	100
(*bug*^{p5bnc})	Outcross [b]	158	0	0
	Backcross [c]	487	35	50

[a]Incross: Each parent was homozygous for the *lrp2* mutation and showed the large eye phenotype.
[b]Outcross: One parent was homozygous for the *lrp2* mutation and showed the eye phenotype. The other parent was wild-type. Five wild-type strains were used for the *lrp2*C23X test crosses, while three wild-type strains were used for the *lrp2*Q413X test crosses.
[c]Backcross: One parent was homozygous for the *lrp2* mutation and showed the large eye phenotype. The other parent was an adult progeny from an Outcross and therefore heterozygous for the *lrp2* mutation.
[d]Some families after repeated incrossing showed 100% penetrance of the large eye phenotype.
doi:10.1371/journal.pgen.1001310.t001

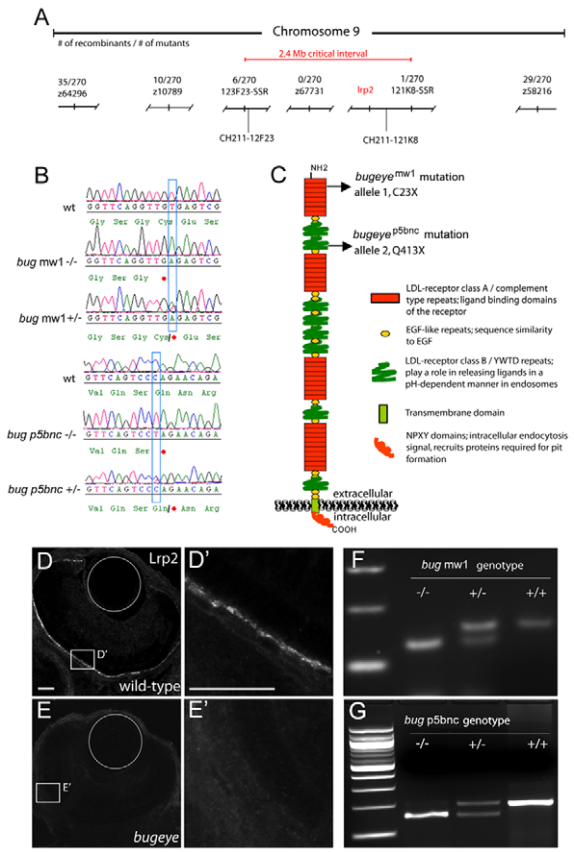

Figure 2. Both *bugeye*^{mw1} and *bugeye*^{p5bnc} mutants have non-sense mutations in *lrp2*. *A* Genetic and corresponding physical map of the critical interval for *bugeye*^{mw1} and *bugeye*^{p5bnc} locus on chromosome 9. Associated number of recombination events per 270 meioses are shown for each polymorphic marker. SSR, Simple sequence repeat. *B* Sequence comparisons of *lrp2* revealed distinct non-sense mutations in *bugeye*^{mw1} and *bugeye*^{p5bnc}. In mw1, the cysteine at amino acid position 23 is changed to a stop codon by a T>A mutation; in p5bnc, the glutamine at 413 is changed to a stop by a C>T mutation. In both, heterozygous genotypes show both alleles. *C* Model of Lrp2 protein structural domains, with the locations of the identified mutations indicated by arrows. The bulk of the protein is extracellular with ligand binding domains, while the intracellular domain contains an NPXY endocytosis sequence motif. *D-E* Immunostaining for Lrp2 in 56-hpf pigmentation-blocked embryos. Lrp2 immunoreactivity was robust in the retina pigmented epithelium (RPE) of wild-types (D), but absent in *bugeye* embryos (E). Insets in D and E are magnified in D′ and E′. Scale bars = 25 µm; circles show placement of the lenses. *F* Images of ethidium bromide stained agarose gels show restriction fragment length polymorphism (RFLP) genotypes: homozygous mutant (−/−), heterozygote (+/−) and wild-type (+/+) genotype for each mutation.
doi:10.1371/journal.pgen.1001310.g002

lrp2 mutants (Figure 3A). Despite individual variability, the average body length growth rates between wild-type and *lrp2* mutant fish were indistinguishable (Figure S3). For the E:B ratio, no wild-type fish had a value greater than 0.05 (most fell between 0.02 and 0.04), and mutants with visibly enlarged eyes had an E:B ratio ≥0.07. The onset of large eyes was variable both within shared tanks of siblings and between generations, but a statistically significant difference between mutant and wild-type fish was consistently found at 2 months (Figure 3A and data not shown). In general, *lrp2* mutant eyes become visibly enlarged in adults between 2–6 months and eye growth often plateaus between 8–12 months.

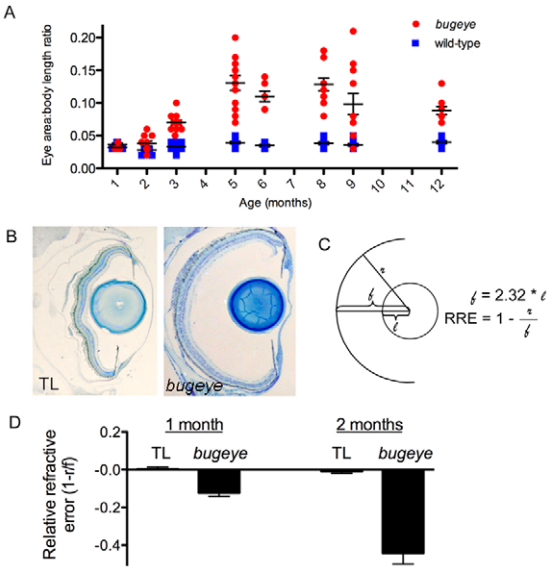

Figure 3. Eye growth and relative refractive errors in *bugeye/lrp2* mutants. *A bugeye* mutants have a greater eye area to body length ratio (E:B) than age-matched wild-types beginning at 2 months ($p<0.05$, t-test), which becomes more pronounced with age. Each dot represents the E:B for an individual eye. *B* Histological transverse sections through the whole eye show an increased depth of the vitreous chamber (from the lens to retina) in *bugeye* (right) as compared to wild-type fish (left). *C* Diagram showing the calculation of relative refractive error (RRE): lens radius (l) and retina radius (r), using a focal length of the lens (f) as 2.32 x lens radius. *D* The RRE measurements revealed mild but significant myopia in 1-month *bugeye* fish ($p=0.0002$, t-test), that becomes more dramatic at 2 months of age ($p<0.0001$, t-test). $n=6$ eyes each for 1 month TL and *bugeye*; $n=16$ and 22 eyes for 2 month TL wild-type and *bugeye*, respectively.
doi:10.1371/journal.pgen.1001310.g003

Histological cross-sections of *lrp2* mutant eyes revealed that the region with the greatest increase in size was the depth of the vitreous chamber (Figure 3B). This suggests that in large-eyed mutants, the retina lies behind the point at which the lens focuses light and the eyes are therefore myopic. We calculated the relative refractive error (RRE), an estimate for the degree of myopia, for *lrp2* mutant eyes relative to wild-type eyes at 1 and 2 months using retina and lens radius measurements collected from histological sections. Using the RRE equation, a myopic eye has a negative value and a hyperopic eye is positive (Figure 3C; Methods). We found that *lrp2* mutant eyes are slightly myopic at 1 month, but become significantly more myopic by 2 months (Figure 3D).

Lrp2 mutants show reduced retinal cell density with increased eye size

Histology suggested retinal cell density was affected in *lrp2* mutant eyes (Figure 4). At 1 month, before eyes of mutant fish were visibly enlarged, there was a small reduction in retinal cell density as compared to wild-type fish (Figure 4A, 4B). By 2 months, when the onset of large eyes had occurred in some mutants but not in others, there was a significant difference in cell density in all layers of the retina (Figure 4C, 4D). As expected, at 6 months when relative eye size was greater overall, there was a further decrease in cell density (Figure 4E, 4F). When considering retinal cell density for each layer as a function of relative eye size (as measured by the ratio of the retinal cross-section length to body length), we found that for mutants, the relation between neuron density and relative eye size decreased in a linear manner (Figure 5A). The same was true when considering just the absolute

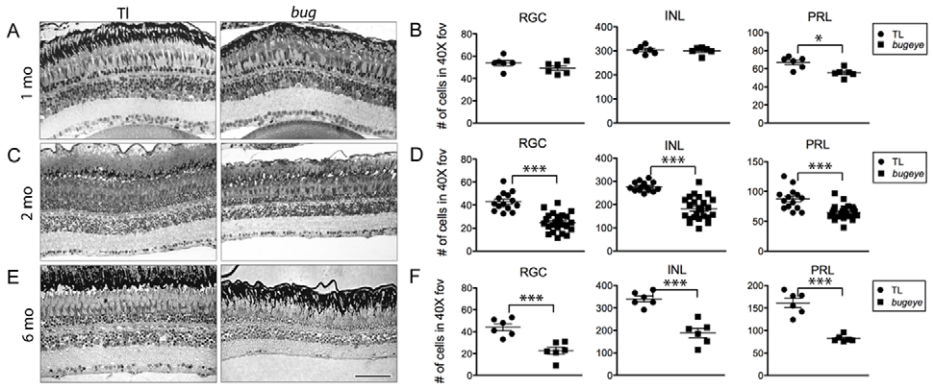

Figure 4. Retinal cell density. Semi-thin plastic sections of the central retina, with associated quantification of cell density in each neural layer at 1 (*A–B*), 2 (*C–D*), and 6 (*E–F*) months in TL and *bugeye*. Scale bar A–E = 50 µm. *p<0.05, ***p<0.001, t-test; FOV, field of view.
doi:10.1371/journal.pgen.1001310.g004

size of eye (as measured by retinal cross-section length, Figure 5B). Interestingly, there was an increase in photoreceptor density in larger eyes for wild-type fish (Figure 5B). When considering cell density for wild-type and mutant eyes of the same absolute size, but of different ages in order to match size, density was still reduced in *lrp2* mutant fish (Figure 5C). For this comparison we evaluated retinal cell density of 6-month old wild-type fish and 2-month old *lrp2* mutant fish, each that had retinal lengths that fell between 2–3 mm. Importantly, there was no significant change in cell density for the retinal ganglion cells layer between 2–6 months in wild-type fish. For the inner nuclear and photoreceptor layers, there was a small, but significant change (ANOVA, $p<0.001$), where the cellular densities increased with age. Together, these data suggest that the reduced neuron density seen in *lrp2* mutant retinas is not simply due to an acceleration of normal ocular growth.

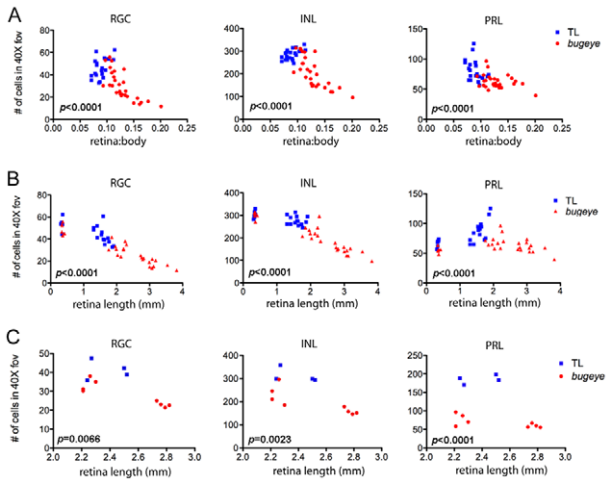

Figure 5. Retinal neuron density in relation to relative and absolute eye size. *A,B* Cell density in 1 and 2-month central retinas versus relative eye size(A), as measured by the retinal cross-section length to body length ratio, or versus absolute eye size (B), as measured by only retinal cross-section length. *C* Cell density in central retinas of similarly sized (2–3 mm retinal cross-section length) TL and *lrp2* mutant eyes. Reported *p*-values (lower left of each graph) are for a Hotelling-Lawley multivariate test comparing the differences between TL and *lrp2* mutants for both cell density and relative eye size (A) or absolute eye size (B, C). In addition, analysis indicated that for TL wild-type fish, retinal length and photoreceptor density (B) approximated a linear relationship (Pearson Correlation Coefficient = 0.77; $p<0.001$).
doi:10.1371/journal.pgen.1001310.g005

Despite the reduced cell density in mutant eyes, total retinal cell number was estimated to be greater than wild-type, owing to the much larger eye size overall. We estimated total retinal cell numbers by considering the retina area as that of the surface area for half a sphere and extrapolated total cell numbers using density data. These calculations showed that mutant eyes with E:B ratios >0.07 had significantly increased numbers of total neurons. More directly, analysis of DNA content, which is proportional to total cell number, confirmed that large-eyed mutant fish (EB ratio >0.07) had more cells, even though retinal cell density was much lower (data not shown).

The altered retinal cell density in *lrp2* mutants could be due to either insufficient cell generation to match scleral growth and remodeling, or through increased cell death. To address these possibilities we analyzed by immunofluorescence the number of proliferating cells within the ciliary margin zone (using Mini-chromosome maintenance homolog 5, Mcm5 antibodies) and the number of apoptotic cells across the retina (using activated-Caspase3 antibodies). Mcm5 is required for DNA replication and is expressed throughout the cell cycle in all proliferating cells, but the protein is rapidly lost in post-mitotic cells. Proteolytic cleavage of Caspase3, recognized by the activated-Caspase3 antibody, is one of the last steps in the apoptosis cascade and marks cells committed to die in a number of contexts, including glaucoma. At 1 month, proliferation in both wild-type and *lrp2* mutant retinas was primarily confined to the ciliary marginal zone, a stem cell niche where ongoing proliferation from multipotent elongated neuroepithelial cells is known to occur in fish [17] (Figure 6A–6C). For each genotype, occasional Mcm5-positive cells were also located in the inner nuclear layer, which have previously been shown to be rod progenitor cells in teleost fish [18–20]. At 2 months, cell counts indicated a reduction in Mcm5-positive cells per CMZ niche in *bugeye* fish, suggesting maintenance of stem cells was inadequate to match eye globe growth (Figure 6D–6F). Consistent with this observation, a role for Lrp2 in maintaining neuronal stem cells of the adult mouse forebrain has been recently described [21].

Similar to analysis of proliferation, cryosections of wild-type and *lrp2* mutant retinas were used to investigate cell death. However, very few dying cells were noted in sections of retina from either condition. Similar results were obtained using the TUNEL assay to characterize dying cells. We therefore used activated-Caspase3 immunoreactivity on control and *lrp2* mutant flat-mounted retinas

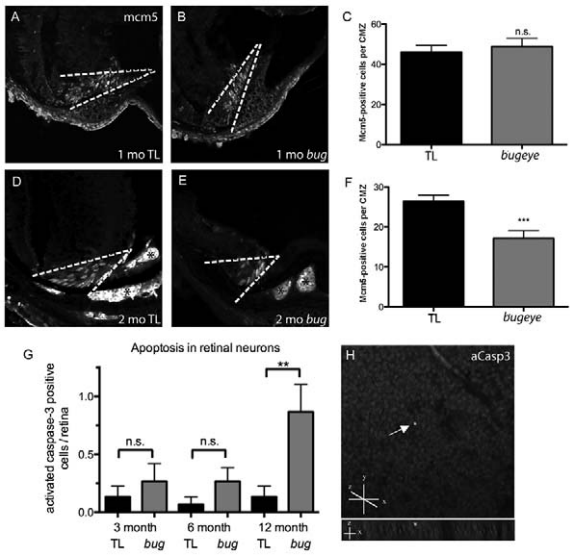

Figure 6. Retinal proliferation and apoptosis. *A–F* Mcm5 expression in 1 (A–C) and 2-month (D–F) cryosections. Dashed white lines denote proliferative ciliary marginal zone (CMZ) of the retina; asterisks indicate autofluorescent blood vessels. *G* Quantitation of apoptotic cells identified on whole retina flat-mounts by activated caspase-3 (aCasp3) immunofluorescence. *H* Confocal images of aCasp3-positive cell in 1 year old *bugeye* mutant. Upper shows compressed z-stacks, lower shows 90°rotation to reveal z location of positive cell (arrow). The flat mounted retinas were orientated with retinal ganglion cell layer up. $n = 15$ eyes for each condition; ***$p<0.001$, **$p<0.01$, n.s., not significant (t-test).
doi:10.1371/journal.pgen.1001310.g006

to observe all neurons from individual samples. Even by flat-mount analysis, there was little apoptosis up to 6 months of age (Figure 6G), although at these times *bugeye* mutants showed trends towards increased numbers of activated-Caspase3-positive cells. By 12 months, apoptosis in *bugeye* retinas was significantly elevated. We also noted that activated-Caspase3 immunoreactivity from all ages was restricted to the retinal ganglion cell layer (Figure 6H). It is possible, however, that some cells, including those outside of the ganglion cell layer die by Caspase3- and TUNEL-independent mechanisms. Overall, these data indicate that initially, as *lrp2* mutant eyes expand, proliferation is not sufficient to maintain proper cell density and later, perhaps following mechanical stress imposed by retinal stretch, retinal ganglion cells begin to die.

Genes associated with retinal ganglion cell stress and axon pathology are upregulated in *lrp2* mutants

In the following studies we evaluated the onset of retinal ganglion cell stress and pathology. Relative expression levels of twelve genes known to be up-regulated in animal models of retinal ganglion cell injury was surveyed by quantitative RT-PCR. This panel of markers included three transcripts expressed in microglia (*aif1l*, [22,23]; *apoeb*, [24,25]; *arg1*, [26,27]), one expressed in Müller glia and astrocytes (*gfap*, [28,29]), and eight expressed in retinal ganglion cells (*atf3*, [30,31]; *c1q*, [32–34]; *c-jun*, [31,35,36]; *gap43*, [37,38]; *klf6a*, [31,39]; *socs3a* and *socs3b*, [31,40,41]; *thy1*, [42,43]). Analysis was conducted on cDNA isolated from pooled 1-month-old retinas, a time just prior to when mutant eyes were measurably enlarged. We chose this early time-point to avoid measuring changes that might simply reflect significant alterations in cell proportions and density. With this assay, we found induction primarily of transcripts associated with retinal ganglion cells, but not for the glia-associated genes (Figure 7A).

To investigate whether the markers of retinal ganglion cell stress correlated with optic nerve pathology, we first compared sagittal sections of wild-type and *lrp2* mutant optic nerve heads from 6-month-old fish by light microscopy. We then analyzed cross-sections of wild-type and *lrp2* mutant optic nerves, just posterior to the optic nerve head from 7- and 12-month-old fish by transmission electron microscopy (TEM). In zebrafish, like other teleost fish as well as some rodents, the optic nerve head is comprised of an astroglial lamina without obvious elastin-collagen rich laminar plates as observed in primates [44–46]. In addition, as the optic nerve exits the fish eye, it is initially unmyelinated, like that in humans and most mammals [47–50]. Histology of the optic nerve head did not reveal excavation or cupping in *lrp2* mutants, but did indicate mutant nerves were larger, consistent with increased total numbers of retinal ganglion cells in the large-eyed fish (Figure 7B). Optic nerve cross-sections for TEM were collected distal to the exit point from the eye within the myelinated region of the optic nerve, which is adjacent to the site of axonal injury in glaucoma [51–53]. Nerve damage was scored as 1) degenerating axons, as noted by electron-dense appearance, 2) axons having an unraveled myelinated sheath, or 3) space left behind by a shrunken and degenerating axon. At both ages, examples for each type of pathology were found in wild-type and *lrp2* mutant optic nerves (Figure 7C). Surprisingly, when total counts were normalized to area (mm^2) there were no differences between genotypes or ages (Figure 7D).

Because the ultrastructural signature of degenerating axons following a crush injury is relatively short-lived in the optic nerve tract of teleost fish as compared to mammals [54], we utilized a genetic tool to label damaged and regenerating axons over a longer period of time [55]. We crossed Tg(3.6Fr*gap43*:GFP)^{mil1} transgenic fish with *lrp2* homozygous mutants and then used the resulting progeny to backcross with non-transgenic *lrp2* mutant fish. This breeding scheme resulted in families with equal proportions of *lrp2* heterozygous and homozygous mutant fish carrying single insertions of the 3.6Fr*gap43*:GFP transgene. This transgene contains 3.6 kb of regulatory sequence (5′ flanking region and first intron) from the *Takifugu rubripes gap43* locus driving GFP. Importantly, in these transgenic fish, GFP is expressed in axons following injury [55]. For our analysis, we compared large-eyed *lrp2* homozygous mutant fish (>0.07 E:B ratio) to normal-eyed heterozygous siblings (Figure 8K–8T). In all large-eyed mutant fish we observed strong activation of GFP in a sub-set of retinal ganglion cells. In the majority of mutant retinas examined (6 of 6 at 6 months, Figure 8P–8T; and 10 of 12 at 12 months, data not shown), there was a characteristic axon 'wandering' and 'circling' around the optic nerve head. This axon phenotype, where GFP-positive axons approached the optic nerve head in a disorganized and circuitous fashion, was never observed in retinas from age matched *lrp2* heterozygotes (Figure 8K–8O) or from 12-month wild-type fish that carried the 3.6Fr*gap43*:GFP transgene (data not shown). The transgene was activated with variability at 2 months in both wild-type or *lrp2* mutant fish (Figure 8A–8J), but the wandering axon phenotype was only rarely observed in mutants at this early timepoint. Weak expression of the transgene was noted in the nerve fiber layer of non-mutant retinas, consistent with the ongoing neurogenesis of zebrafish. In addition, older wild-type fish occasionally showed stronger GFP-positive axons, suggesting sporadic age-related degeneration. In wild-type eyes, all of the low-GFP expressing axons, as well as the occasional high-GFP expressing axons, exited the eye directly without wandering or circling the optic nerve head like those of mutants. To address

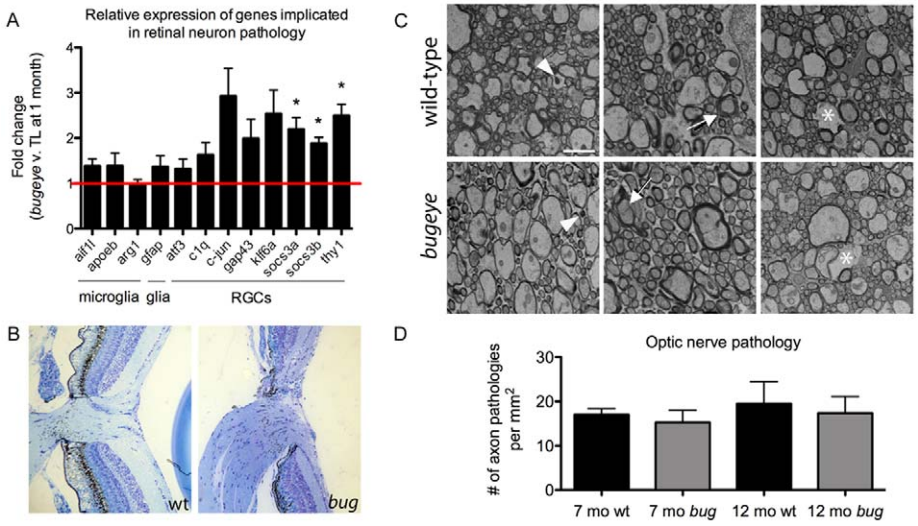

Figure 7. Analysis of retinal and optic nerve head pathology. *A* The relative expression levels of genes previously associated with retinal neuron pathology measured by real-time PCR on cDNA made from RNA isolated from the eyes of 1-month TL and *bugeye* fish. The cell populations that predominantly express the marker genes are listed below the bar graph. $n = 4$ independent samples of 6 pooled eyes each from TL wild-type and *bugeye* mutant fish. Error bars show standard error of the mean; *$p<0.05$. *B* Histological cross sections through the optic nerve head in TL wild-type (left) and *bugeye* (right) samples a 6 months of age. *C* Representative electron micrographs showing each type of axon pathology observed in cross-sections of TL wild-type (top) and *bugeye* (bottom) optic nerves. Arrowheads (left), degenerating axon; arrows (middle), unraveling myelin sheath; asterisks (right), lost axon. Scale bar = 2 μm. *D* Quantification of the optic nerve ultrastructure analysis reported as number of axon pathologies per mm^2. $n = 6$ and 7 nerves for 7- and 12-month TL wild-type, respectively; $n = 8$ nerves each for 7- and 12-month *bugeye*.
doi:10.1371/journal.pgen.1001310.g007

whether the chronic stress conditions of *lrp2* mutants differ from acute injury, we performed optic nerve crushes on adult *gap43*:GFP fish. At 6 days post-crush there was significant up-regulation of GFP across the retina (Figure S4). By 5 weeks post-crush, when axons had regrown [56], there was only an occasional wandering axon. Most samples following nerve crush, however, showed accurate and direct axon targeting through the optic nerve head. By 11 weeks post-crush, there was significant reduction in transgene activation and no axons showed wandering or circling at the optic nerve head like age-matched *lrp2* mutants. This comparison highlights the differences between the chronic stresses caused by the *lrp2* mutation versus the acute, crush injury model, in which the genetic model results in changes at the optic nerve head that are not evident in the post-nerve head crush paradigm.

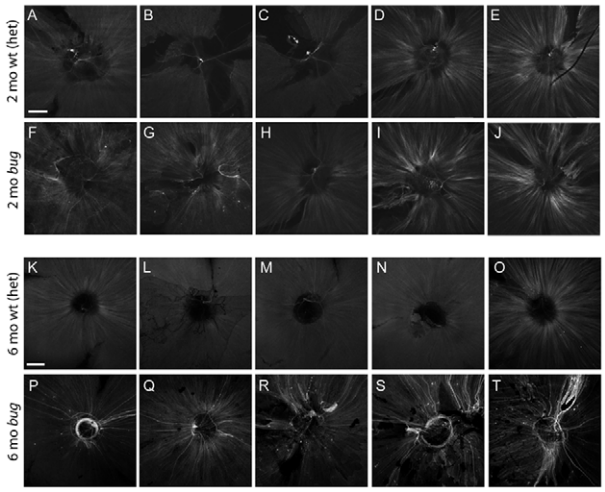

Figure 8. Expression of the *gap43*:GFP transgene in *lrp2* mutants. *A–L* Expression of the *gap43*:GFP transgene in flat-mounted retinas from 2-month *bugeye* heterozygotes (wild-type) (A–E) and homozygous mutants (F–J). Shown are 5 representative samples for each condition. Images capture a single plane of the nerve fiber layer using equal gain settings on a confocal microscope. Scale bar = 200 μm. Similar analysis on 6-month *bugeye* heterozygotes (wild-type) (K–O) and homozygous mutants (P–T). Note the stronger activation and unique wandering/circling phenotype in mutant axons.
doi:10.1371/journal.pgen.1001310.g008

Discussion

A major challenge with research on either myopia or glaucoma is identifying genetic lesions that impact the diseases. Recently, genome wide association studies for both diseases revealed non-coding associated changes, but the predicted effects on phenotypes were small and the actual gene products affected by the intergenic alterations have yet to be identified [57–59]. In addition to defining genetic susceptibilities for glaucoma, there is a need to understand and model how other risk factors like age, raised IOP, and myopia itself affect the onset, severity, and progression of neuropathology. In our studies we identified non-sense mutations in zebrafish *lrp2* that lead to phenotypes that are known risk factors for glaucoma. These phenotypes included increased IOP, enlarged eye globes with significant refractive errors, decreased retinal neuron density, activation of retinal ganglion cell stress genes, and distinct axon pathology at the optic nerve head. The zebrafish *lrp2* mutants have similar heritable phenotypes to the black moor goldfish [60,61] and the RCS;rdy- rat [62]. It will be interesting to see if *lrp2* or pathway genes are affected in either of those models. Similarly, it is possible that alterations to genes that control pathways affected by loss of Lrp2 might influence myopia or forms of glaucoma. To date, however, polymorphisms in Lrp2 have only been linked with urate and cholesterol levels in serum [63,64] and the molecular and cellular pathways affected by loss of Lrp2 that impact the ocular phenotypes remain uncharacterized. In general,

Lrp2 functions in regulation and homeostasis of multiple bioactive molecules including vitamins, hormones, nutrients, and growth factors through localized tissue delivery or reuptake by epithelia. In knowing the affected gene, the zebrafish mutants hold promise in shedding light on how de-regulated signaling and homeostasis affect phenotypes such as elevated IOP or excessive eye growth.

While it is tempting to speculate that the excessive eye growth in *lrp2* mutants is due to the elevated IOP, our studies do not rule out the possibility that these two phenotypes are distinct. In fact, the only two Donnai-Barrow patients who have had their IOPs reported (each with non-sense mutations in *LRP2*), showed values in the normal range [65]. Despite normal IOPs, the eyes of the two young siblings were enlarged and showed high myopia. Furthermore, as an endocytic receptor found on the RPE, Lrp2 is an interesting candidate as a direct regulator of emmetropization [66]. Potentially, Lrp2 mediates the availability or transport of signaling molecules from the retina to affect remodeling within the sclera. In this context Lrp2 might be key in facilitating the matching of visual input with axial length of the eye. Nonetheless, relationships between eye pressure and size are established and the elevated IOP in zebrafish *lrp2* mutants is likely to be at least contributory to the observed buphthalmia. Consistent with this possibility, in the few mutant fish where the eye phenotype presented in a unilateral manner, IOPs were normal in unaffected eyes, yet elevated in enlarged ones. Indeed, expression of Lrp2 on the ciliary epithelium suggests a direct role in IOP regulation, particularly considering the function of Lrp2 at other sites of fluid regulation. For example in mice, Lrp2 has been shown to regulate glomerular filtration in the proximal tubule of the kidney and in the choroid plexus the receptor modulates homeostasis of cerebrospinal fluid [67–71].

A significant characteristic of *lrp2* mutant fish is the strong relationship between abnormal eye globe growth, retinal thinning, and activation of retinal ganglion cell stress markers. In this context, *lrp2* mutants have value as a genetic model for studying the effects of protracted mechanical stress on retinal ganglion cells, their axons, and the associated glia. As this phenotype relates to glaucoma, it was surprising that mutant fish did not show significantly elevated optic nerve pathology with TEM analysis. It is possible that the stresses induced by *lrp2* mutations simply do not reach a threshold to cause ultrastructural pathology. Alternatively, low-grade stress may actually "pre-condition" and promote protective mechanisms in the mutant neurons [72,73]. However, the lack of a difference in ultrastructure pathology between mutant and wild-type siblings could also be explained by the surprisingly high number of pathological events noted in the wild-type fish. This perhaps relates to the regenerative capacity of teleosts [56,74] and a relaxation of selective pressure to maintain nerve health with normal aging. Through evolution, fish may have lost highly-robust nerve protective mechanisms against age-related stresses, and instead rely on ongoing growth and regeneration to maintain vision, perhaps accounting for the unexpected pathology scored in wild-type optic nerves. In addition, because a higher proportion of the ganglion cell axons in *lrp2* mutant fish are in fact younger than those of wild-type siblings (due to the excessive ongoing generation of neurons in their eyes), many of the optic nerve profiles might be expected to in fact look healthier in a relative manner.

The modest death of retinal ganglion cells in *lrp2* mutants was less surprising. First, extended retinal ganglion cell soma survival, despite axonal damage and dysfunction, is known for the DBA/2 mouse glaucoma model. DBA/2 mice show a pigment dispersion-related glaucoma with elevated IOP [75,76]. In young DBA/2 mice, axons at the nerve head often show focal insults with many having dystrophic features [51]. In many aged animals, axons are clearly degenerative [51]. Most retinal ganglion cells, however, survive for extended periods of time and their disconnected proximal (intra-retinal) axons take on reactive and stressed characteristics [51,77,78]. Second, the resilient nature of retinal ganglion cells in teleosts has been well characterized. In fact for goldfish, experimental axotomy or optic nerve crush results in less than 10% death of retinal ganglion cells [79], and in zebrafish only 20% of the lesioned neurons are reported to die [80]. In contrast, optic nerve axotomy in mammals results in apoptosis of nearly all retinal ganglion cells [81–83]. The regrowth of axons in teleosts occurs over a course of weeks and results in correct axon pathfinding and appropriate tectal innervation [84,85]. In contrast, in *lrp2* mutants, retinal ganglion cells appear to be under prolonged mechanical stress from the stretching and growth of the eye globe. This was evident from the changes in retinal density with eye enlargement and the activation of retinal ganglion cell stress markers. Of interest, axon regrowth through the optic nerve was affected in *lrp2* mutants. The wandering and circling phenotype of the *gap43*:GFP axons in large-eyed mutants is reminiscent of the EphB3-dependent 'reactive plasticity' following optic nerve injury in mice [86,87]. Regardless, of why *bugeye/lrp2* mutants do not show dramatic retinal ganglion cell death, this fact emphasizes that while these fish model initiating risk factors for glaucoma, they do not model the end stages of the disease.

Lrp2 mutations in humans and mice are often lethal, but always developmentally relevant, particularly within the nervous system [71,88,89]. Our analyses of both *bugeye* alleles indicate Lrp2 is dispensable for survival in zebrafish. Furthermore, we did not detect morphological phenotypes in mutant embryos, similar to the observations following oligonucleotide knock-down of zebrafish *lrp2* [67]. The total lack of lethality in zebrafish *lrp2* mutants may be due to species differences in respiration, as mice mutants often die from respiratory failure at birth. Alternatively, there may be compensation from other Lrp family members in zebrafish. Compensation from Lrp family members may also explain the lack of obvious developmental defects. More detailed studies of the zebrafish mutant embryos and larvae are warranted to assess whether subtle defects exist.

In summary, we have identified mutations in *lrp2* that cause adult-onset ocular pathogenesis in zebrafish. While mutants appear normal during larval stages of development, as young adults they develop enlarged eyes with elevated IOP. Over time, retinal cell density becomes significantly reduced due to insufficient proliferation of marginal zone stem cells and increased neuronal cell death. Markers of retinal ganglion cell stress become elevated and damaged and/or regenerating axons at the optic nerve head show a characteristic wandering and circling phenotype. These fish will be valuable for future studies on the signaling and cellular mechanism of myopia and other risk factors for glaucoma.

Materials and Methods

Fish maintenance

Wild-type and mutant zebrafish (*Dano rerio*) were maintained at 28°C with a 14 on/10 off light cycle and were feed a standard diet [90]. All animal husbandry and experiments were approved and conducted in accordance with the guidelines set forth by the Institutional Animal Care and Use Committee of the Medical College of Wisconsin.

Mutant and transgenic alleles

bugeye; *lrp2*^{mw1} (this study)
bugeye; *lrp2*^{p5bnc} (this study)
Tg(3.6Fr*gap43*:GFP)^{mil1} [55]

Accession numbers

lrp2, HM_754616
aif1l, NM_198870
apoeb, NM_131098
arg1, XM_001922563
gfap, NM_131373
atf3, NM_200964
c1q, NM_001005976
c-*jun*, NM_199987
gap43, NM_131341
klf6a, NM_201461
socs3a, NM_199950
socs3b, NM_213304
thy1, NM_198065

Measurement of intraocular pressures

Servo-null electrophysiology was used to measure IOPs as described previously [14].

Recombinant linkage mapping

Mapping panels of 6 month adult mutant fish (obviously enlarged eyes) were collected from backcross pedigrees. Bulked segregant analysis, using pooled samples of mutant genomic DNA and individual parental DNA, was conducted with simple sequence repeat (SSR) markers to establish linkage to Chromosome 9. For higher-resolution mapping, sequencing of parental genomic DNA in regions associated with the closest linked microsatellite markers was done to find additional SSRs. These new SSRs were then used to refine the critical interval by analyzing single mutant fish.

Genotyping

PCR was performed on DNA isolated using the Puregene kit (Qiagen, Germantown, MD) from tailfin-clips, using primers designed to amplify the allele specific mutations in *lrp2*:

bug mw1 F: CGTTATTTTCTGTCTAGGTTCAG**G**TTA,

bug mw1 R: GAAAAGAAAAGATTGATACATACGG

bug p5bnc F: GTGTGTTTTCTGAAAACTGTCAAGC,

bug p5bnc R: CTTTGCAGCTGGTAATGAAAATCCACAC-CAACAGCGGCTCCTCTGT**C**CTA. Underlined letter in primer denotes mutant nucleotide, bolded letter denotes a single nucleotide change in the primer to generate a novel restriction site for each allele (*bug* mw1: MseI; *bug* p5bnc AvrII).

Eye size and body length measurements

Fish were anesthetized with 0.05% Tricaine and body lengths were measured in side-view from the tip of the head to the end of the trunk (before the caudal fin). To measure eye size, anesthetized fish were imaged at a fixed magnification from a dorsal perspective using a Nikon CoolPix995 camera attached to a Leica MZFLIII microscope. These images were imported into Metamorph software (Universal Imaging Corp, Philadelphia, PA), and the area of each eye from the dorsal view was traced using the Region Measurements function.

Relative refractive error

Lens radius (L) was measured from histological cross sections; retina radius (R) was back-calculated by assuming the retina to be a semi-circle, measuring the length of the retina, and taking that measurement as half the circumference of a circle (so R = length of retina/π). Sections with minimal distortion from processing were used and no attempts to correct for distortions were made. A focal length (F) of 2.32 x L for the lens was used as in studies with goldfish [91]. RRE was calculated as 1- (R/F). By this calculation, all wild type fish were predicted to be slightly hyperopic (RRE >1), likely due to fixation artifact. To adjust this, the ratio of (R/F) was multiplied by a constant factor for both genotypes at each age (1 month, 1.15; 2 months, 1.18), so that on average, the wild type fish were emmetropic (RRE = 0).

Histology

Heads were removed from terminally anesthetized fish and fixed overnight in gluteraldehyde/paraformaldehyde at 4°C, washed three times in PBS, and dehydrated in increasing ethanol solutions (50%, 70%, 80%, 90%, 95%, 100%, 100%, 100%) for 10 minutes each, all at RT. The heads were then infiltrated with propylene oxide for 15 minutes twice, then a 1:1 mix propylene oxide:epon for 2 hours at RT. An additional equal volume of epon was added to the samples and these were incubated overnight with culture tube caps off so that the propylene oxide would evaporate. Heads were bisected when necessary to fit in block-molds, embedded in epon, and baked for at least 24 hours at 65°C. Semi-thin sections were cut on a Leica RM2255 microtome and stained with 1% Toluidine, 1% Borax.

Cell counts

For each eye, 5 non-consecutive sections were imaged from the central retina (sections with the largest lens diameter) with a 40X objective on a Nikon E600FN microscope with a Photometrics CoolSnap camera attached. Each image was printed and the nuclei in each layer of the retina were counted. The average of the 5 sections was calculated and represented 1 data point. For sample condition, between 6–12 eyes were scored in this manner.

Immunostaining

Zebrafish embryos or isolated eyes were fixed overnight at 4°C in 4% PFA (pH 7.4, in PBS), washed three times for 10 minutes in PBS, then infiltrated with increasing concentrations of sucrose (15%, 30%) for 2 hours each at 4°C, followed by overnight incubation in HistoPrep freezing media (Fischer Scientific, Pittsburgh, PA). Cryoprotected embryos were embedded in HistoPrep and flash frozen, sectioned at 10–12 µM and collected on Supercharge Plus slides (Fischer Scientific). Cryosections were allowed to dry on the slide for 1hr at RT, and the edge of the slide was traced with a PAP pen. Slides were rinsed briefly with PBTD (PBS +1% DMSO +1% Tween-20) to rehydrate the tissue, and then incubated in block (5% donkey serum in PBTD) for 2 hours at RT. Primary antibody was diluted in block (Sheep-anti-Lrp2 1:1000, gift from Dr. Thomas Willnow (Max Delbruck Center, Berlin, Germany)) and incubated on slides overnight at 4°C. Antibody was removed and slides were washed three times with PBTD rinses, and secondary antibody diluted in block (Cy3-Donkey anti-Sheep 1:250, Jackson ImmunoResearch, Westgrove, PA) was incubated at RT for 1.5 hours. Secondary antibody was removed with three washes of PBTD, and slides were mounted in 1:1 PBS to glycerol with 0.1% Hoechst nuclear stain (cryosections). Images were collected using a Nikon C1 confocal microscope. The same procedure was followed for dissected whole adult retinas prior to flat-mount analysis, using anti-cleaved caspase-3 primary antibody (1:500, Cell Signaling

Technology, Danvers, MA) and DyLight 488 secondary (1:1000, Jackson ImmunoResearch).

Real-time PCR

1 month fish measuring between 10–12mm were anesthetized in Tricaine, and both eyes were removed and placed immediately in TRIzol (Invitrogen). Each sample was a pool of 3 pairs of eyes (6 eyes per sample), and 4 samples were used for each genotype. RNA was isolated following the Invitrogen protocol. Reverse-transcription PCR was carried out following the protocol for SuperScript III First Strand Synthesis (Invitrogen). Gene specific primers were used as follows to amplify the genes of interest: Aif1l (F: CAACATGGACTTACAAGGCG, R: TCCTCTTCGTC-TCTGTACTTCTG); ApoEb (F: GTGCAAAACATCAAGG-GCTC, R: GGGTCATCTGGGTTTGGAG); Arg1 (F: TGG-GCATCAAAACCTTCTCC, R: AAACTCAGATGGATCGG-CTTC); Atf3 (F: AGCCTGCATGAACACTGAG, R: TTTT-CCTTCGGTCGTTCTCC); C1q (F: CTCTGCTGACACCT-GTCCTG, R: GGTGGTCCTTTCAGACCAAA); c-Jun (F: ACGTGGGACTTCTCAAACTG, R: TCTTGGGACACAGA-AACTGG); Gap43 (F: GAAGGCAATGCACAGAAAGAG, R: TGCTGGTTTGGATTCCTCAG); Gfap (F: AAGCTCTGC-AAGACGAGATC, R: GCTTAGACACATCCAGATCCAC); Klf6 (F: CACTTAAAAGCACATCAGCGG, R: GAAGTGT-CGGGTTAGCTCATC); Socs3a (F: CATTCAACAAAAGA-GACTCATAGGC, R: TGTGGGTTATCATGGCGATAC); Socs3b (F: CCCAAGATTGAGTCGGATAACG, R: ACCAA-CACAAAGCCCAGAG); Thy-1 (F: CCGGTGTCAATCATT-CAAACTG, R: CAGTGGGAAAGTGAGGAAGG). Initially, PCR products were amplified with Accuprime Taq HighFidelity (Invitrogen), and sequenced to verify specificity. Real-time analysis was performed on a Bio-Rad iCycler using iQ SYBR Green SuperMix (Bio-Rad). 3-step PCR with a 57°C annealing temperature was used for all primer sets except Arg1, Atf3, and Thy1, which used a 2-step PCR with a 54°C annealing temperature to eliminate a non-specific product. All samples were run in triplicate, and fold change was calculated using the ΔΔCt method, with Ef1α as the housekeeping gene for all primer sets.

TEM of optic nerves

Heads were removed from terminally anesthetized fish. In a Petri dish filled with buffer, the optic nerves were dissected from the heads first by removing the skin, skeleton, and connective tissue, leaving the eyes and attached nerves and tectum intact. The tectum was cut from the nerves, leaving the nerves intertwined at the chiasm. The nerves were separated by gently pulling on the eye globes with forceps, and making a cut with an 8 mm Spring Scissors (Fine Science Tools) when necessary. Dissected nerves with attached eyes were then incubated overnight at 4°C in gluteraldehyde/paraformaldehyde fixative. Heads were washed three times in 0.1M PO_4 buffer, and then most of the eye globe removed by using the 8 mm scissors to make a circumferential cut around the optic nerve head, leaving a small portion of the posterior eye attached to the dissected nerve. The nerves were post-fixed in gluteraldehyde/paraformaldehyde for 1 hr at room temperature, washed 3X in 0.1M PO_4 buffer, fixed in 1% buffered Osmuium for 1 hr on ice, and washed 3X with ice cold water. The following steps were all done at room temperature: nerves were dehydrated in an increasing series of MeOH (30%, 50%, 70%, 95%, 100%, 100%, 100%), then infiltrated with acetonitrile, 2X for 15minutes each, followed by 2 hours in a 1:1 mix of acetonitrile and EM Epon, and finally incubated in 100% EM Epon overnight, embedded in molds, and baked for at least 24 hours at 65°C. The blocks were trimmed to between 100–200 microns past the optic nerve head on a Leica RM2255 microtome, and ultra-thin sections were cut and plated on a grid, and imaged using a Hitachi H600 transmission electron microscope. The entire nerve cross-section was canvassed at 8000X, and 10–16 representative images were collected from each nerve at this magnification. Quantitative assessment of nerve pathology was conducted in a double-blinded manner in which both the TEM microscopist and the individual scoring pathology for the samples was unaware of the sample genotype.

Retinal flat-mount analysis

Eyes were dissected from terminally anesthetized adult fish and fixed overnight at 4°C in 4% PFA (pH 7.4, in PBS), then washed three times in PBS. In a Petri dish filled with PBS, a circumferential cut was made at front of the eye with a scalpel, near the border of the anterior and posterior segments. The anterior segment was discarded, followed by removal of the sclera from the posterior segment. The remaining retina with RPE was post-fixed 1-2 hrs with 4% PFA (pH 7.4, in PBS), washed in PBS, and then laid flat on a slide by making incisions through the retina so that it would lay flat. Whole retinas were mounted on the slides with 20 µl of Vectashield Mounting Medium (Vector Labs, Burlingame, CA), and coverslipped. For retinas used for anti-activated-caspase-3 immunofluorescence, antibody incubations were done after removal of the anterior segment and sclera, but prior to flat-mount analysis.

Supporting Information

Figure S1 *A-G bugeye* mutants show varying degrees of asymmetry in eye size (B-G), with the smaller of the two eyes only occasionally falling within the range of the wild-type eye size to body length ratio (E:B; wild-type E:B < 0.05, *bugeye* E:B >0.06). For each eye, the E:B is indicated. *H* In asymmetric eyes of *bugeye* fish, intraocular pressure (IOP) was elevated only in the enlarged eyes. In TL wild-type, the eye measured for IOP first had a higher value than the second eye measured in the same fish. Black symbols represent the first eye of a fish that was measured for IOP and gray symbols represent the second eye. The vertical bar connecting symbols shows eyes from the same fish. Circles represent normal sized eyes; squares represent enlarged eyes.
Found at: doi:10.1371/journal.pgen.1001310.s001 (0.81 MB TIF)

Figure S2 Iridocorneal angle histology of 2.5 month old wild-type (A-,D), normal eyed *bugeye* mutants (B-E), and large-eyed *bugeye* mutants (C-F). *A-C.* Dorsal ciliary epithium. *D-F*, ventral canalicular outflow pathway. Red boxes show from where high magnification isets were derived. Scale bar = 50 µm. Insets are magnified 2.5X. Note the elongated and dysplasic ciliary epithelial cells in B and C insets.
Found at: doi:10.1371/journal.pgen.1001310.s002 (1.18 MB TIF)

Figure S3 Body length measurements over time. Five TL wild-type and *bugeye* fish were measured weekly from 5 to 26 weeks, and again at 30, 35, and 40 weeks. Mean and standard error of the mean (error bars) are plotted for each genotype at all timepoints. Bonferonni tests at each timepoint show that there is no statistical difference between genotypes at any time.
Found at: doi:10.1371/journal.pgen.1001310.s003 (0.13 MB TIF)

Figure S4 Expression of the *gap43*:GFP transgene following optic nerve crush in adult (6 month old) wild-type fish. *A-F* Expression of the *gap43*:GFP transgene in experimental eyes 6 days after optic nerve crush (A-D) or in the contralateral uncrushed control eye (E-F). *G-L* Expression of the *gap43*:GFP transgene in experimental eyes 5 weeks after optic nerve crush (I-

L) or in the contralateral uncrushed control eyes (M-P). *M-R* Expression of the *gap43*:GFP transgene in experimental eyes 11 weeks after optic nerve crush (Q-T) or in the contralateral uncrushed control eyes (E-F). Shown are 3 representative samples for each condition. Images capture a single plane of the nerve fiber layer using equal gain settings on a confocal microscope. Scale bar = 200μm.
Found at: doi:10.1371/journal.pgen.1001310.s004 (1.16 MB TIF)

Acknowledgments

The *bugeye* mw1 allele was originally isolated is a genetic screen conducted in John E. Dowling's laboratory (Harvard University). We thank Clive Wells (MCW) and Michael Cliff for technical assistance with electron microscopy and animal husbandry, respectively. We gratefully acknowledge Drs. Qun Xiang and Sergey Tarima for statistical consultation. We also thank Drs. Thomas Willnow and Salim Abdelilah-Seyfried (Max Delbrueck Center, Berlin) for sharing reagents and for helpful discussions.

Author Contributions

Conceived and designed the experiments: KNV RFC SWMJ RGG BAL. Performed the experiments: KNV JRW RFC MPG GBW RSS SWMJ BAL. Analyzed the data: KNV JRW RFC GBW RSS SWMJ RGG BAL. Contributed reagents/materials/analysis tools: KNV JRW RFC DSW MCM AJU RGG BAL. Wrote the paper: KNV BAL.

References

1. Gehrs KM, Jackson JR, Brown EN, Allikmets R, Hageman GS (2010) Complement, age-related macular degeneration and a vision of the future. Arch Ophthalmol 128: 349–358.
2. Bloom RI, Friedman IB, Chuck RS (2010) Increasing rates of myopia: the long view. Curr Opin Ophthalmol 21: 247–248.
3. Young TL (2009) Molecular genetics of human myopia: an update. Optom Vis Sci 86: E8–E22.
4. Loyo-Berrios NI, Blustein JN (2007) Primary-open glaucoma and myopia: a narrative review. Wmj 106: 85–89, 95.
5. Libby RT, Gould DB, Anderson MG, John SW (2005) Complex genetics of glaucoma susceptibility. Annu Rev Genomics Hum Genet 6: 15–44.
6. Boland MV, Quigley HA (2007) Risk factors and open-angle glaucoma: classification and application. J Glaucoma 16: 406–418.
7. May P, Woldt E, Matz RL, Boucher P (2007) The LDL receptor-related protein (LRP) family: an old family of proteins with new physiological functions. Ann Med 39: 219–228.
8. Fisher CE, Howie SE (2006) The role of megalin (LRP-2/Gp330) during development. Dev Biol 296: 279–297.
9. Christensen EI, Birn H (2002) Megalin and cubilin: multifunctional endocytic receptors. Nat Rev Mol Cell Biol 3: 256–266.
10. Kantarci S, Al-Gazali L, Hill RS, Donnai D, Black GC, et al. (2007) Mutations in LRP2, which encodes the multiligand receptor megalin, cause Donnai-Barrow and facio-oculo-acoustico-renal syndromes. Nat Genet 39: 957–959.
11. Donnai D, Barrow M (1993) Diaphragmatic hernia, exomphalos, absent corpus callosum, hypertelorism, myopia, and sensorineural deafness: a newly recognized autosomal recessive disorder? Am J Med Genet 47: 679–682.
12. Pober BR, Longoni M, Noonan KM (2009) A review of Donnai-Barrow and facio-oculo-acoustico-renal (DB/FOAR) syndrome: clinical features and differential diagnosis. Birth Defects Res A Clin Mol Teratol 85: 76–81.
13. Xu L, Wang Y, Wang S, Wang Y, Jonas JB (2007) High myopia and glaucoma susceptibility the Beijing Eye Study. Ophthalmology 114: 216–220.
14. Link BA, Gray MP, Smith RS, John SW (2004) Intraocular pressure in zebrafish: comparison of inbred strains and identification of a reduced melanin mutant with raised IOP. Invest Ophthalmol Vis Sci 45: 4415–4422.
15. Gray MP, Smith RS, Soules KA, John SW, Link B (2009) The aqueous humor outflow pathway of zebrafish. Invest Ophthalmol Vis Sci.
16. Soules KA, Link BA (2005) Morphogenesis of the anterior segment in the zebrafish eye. BMC Dev Biol 5: 12.
17. Raymond PA, Barthel LK, Bernardos RL, Perkowski JJ (2006) Molecular characterization of retinal stem cells and their niches in adult zebrafish. BMC Dev Biol 6: 36.
18. Johns PR, Fernald RD (1981) Genesis of rods in teleost fish retina. Nature 293: 141–142.
19. Morris AC, Scholz TL, Brockerhoff SE, Fadool JM (2008) Genetic dissection reveals two separate pathways for rod and cone regeneration in the teleost retina. Dev Neurobiol 68: 605–619.
20. Otteson DC, D'Costa AR, Hitchcock PF (2001) Putative stem cells and the lineage of rod photoreceptors in the mature retina of the goldfish. Dev Biol 232: 62–76.
21. Gajera CR, Emich H, Lioubinski O, Christ A, Beckervordersandforth-Bonk R, et al. (2010) LRP2 in ependymal cells regulates BMP signaling in the adult neurogenic niche. J Cell Sci 123: 1922–1930.
22. Bosco A, Inman DM, Steele MR, Wu G, Soto I, et al. (2008) Reduced retina microglial activation and improved optic nerve integrity with minocycline treatment in the DBA/2J mouse model of glaucoma. Invest Ophthalmol Vis Sci 49: 1437–1446.
23. Schluesener HJ, Seid K, Meyermann R (1999) Effects of autoantigen and dexamethasone treatment on expression of endothelial-monocyte activating polypeptide II and allograft-inflammatory factor-1 by activated macrophages and microglial cells in lesions of experimental autoimmune encephalomyelitis, neuritis and uveitis. Acta Neuropathol 97: 119–126.
24. Ignatius MJ, Gebicke-Harter PJ, Skene JH, Schilling JW, Weisgraber KH, et al. (1986) Expression of apolipoprotein E during nerve degeneration and regeneration. Proc Natl Acad Sci U S A 83: 1125–1129.
25. Kuhrt H, Hartig W, Grimm D, Faude F, Kasper M, et al. (1997) Changes in CD44 and ApoE immunoreactivities due to retinal pathology of man and rat. J Hirnforsch 38: 223–229.
26. Pernet V, Bourgeois P, Di Polo A (2007) A role for polyamines in retinal ganglion cell excitotoxic death. J Neurochem 103: 1481–1490.
27. Zhang W, Baban B, Rojas M, Tofigh S, Virmani SK, et al. (2009) Arginase activity mediates retinal inflammation in endotoxin-induced uveitis. Am J Pathol 175: 891–902.
28. Osborne NN, Block F, Sontag KH (1991) Reduction of ocular blood flow results in glial fibrillary acidic protein (GFAP) expression in rat retinal Muller cells. Vis Neurosci 7: 637–639.
29. Tanihara H, Hangai M, Sawaguchi S, Abe H, Kageyama M, et al. (1997) Up-regulation of glial fibrillary acidic protein in the retina of primate eyes with experimental glaucoma. Arch Ophthalmol 115: 752–756.
30. Takeda M, Kato H, Takamiya A, Yoshida A, Kiyama H (2000) Injury-specific expression of activating transcription factor-3 in retinal ganglion cells and its colocalized expression with phosphorylated c-Jun. Invest Ophthalmol Vis Sci 41: 2412–2421.
31. Veldman MB, Bemben MA, Thompson RC, Goldman D (2007) Gene expression analysis of zebrafish retinal ganglion cells during optic nerve regeneration identifies KLF6a and KLF7a as important regulators of axon regeneration. Dev Biol 312: 596–612.
32. Kuehn MH, Kim CY, Ostojic J, Bellin M, Alward WL, et al. (2006) Retinal synthesis and deposition of complement components induced by ocular hypertension. Exp Eye Res 83: 620–628.
33. Stasi K, Nagel D, Yang X, Wang RF, Ren L, et al. (2006) Complement component 1Q (C1Q) upregulation in retina of murine, primate, and human glaucomatous eyes. Invest Ophthalmol Vis Sci 47: 1024–1029.
34. Stevens B, Allen NJ, Vazquez LE, Howell GR, Christopherson KS, et al. (2007) The classical complement cascade mediates CNS synapse elimination. Cell 131: 1164–1178.
35. Herdegen T, Bastmeyer M, Bahr M, Stuermer C, Bravo R, et al. (1993) Expression of JUN, KROX, and CREB transcription factors in goldfish and rat retinal ganglion cells following optic nerve lesion is related to axonal sprouting. J Neurobiol 24: 528–543.
36. Koistinaho J, Hokfelt T (1997) Altered gene expression in brain ischemia. Neuroreport 8: i- viii.
37. Bormann P, Zumsteg VM, Roth LW, Reinhard E (1998) Target contact regulates GAP-43 and alpha-tubulin mRNA levels in regenerating retinal ganglion cells. J Neurosci Res 52: 405–419.
38. Doster SK, Lozano AM, Aguayo AJ, Willard MB (1991) Expression of the growth-associated protein GAP-43 in adult rat retinal ganglion cells following axon injury. Neuron 6: 635–647.
39. Moore DL, Blackmore MG, Hu Y, Kaestner KH, Bixby JL, et al. (2009) KLF family members regulate intrinsic axon regeneration ability. Science 326: 298–301.
40. Fischer D, Petkova V, Thanos S, Benowitz LI (2004) Switching mature retinal ganglion cells to a robust growth state in vivo: gene expression and synergy with RhoA inactivation. J Neurosci 24: 8726–8740.
41. Rolls A, Cahalon L, Bakalash S, Avidan H, Lider O, et al. (2006) A sulfated disaccharide derived from chondroitin sulfate proteoglycan protects against inflammation-associated neurodegeneration. Faseb J 20: 547–549.
42. Dabin I, Barnstable CJ (1995) Rat retinal Muller cells express Thy-1 following neuronal cell death. Glia 14: 23–32.
43. Schlamp CL, Johnson EC, Li Y, Morrison JC, Nickells RW (2001) Changes in Thy1 gene expression associated with damaged retinal ganglion cells. Mol Vis 7: 192–201.
44. Koke JR, Mosier AL, Garcia DM (2010) Intermediate filaments of zebrafish retinal and optic nerve astrocytes and Muller glia: differential distribution of cytokeratin and GFAP. BMC Res Notes 3: 50.
45. Levine RL (1989) Organization of astrocytes in the visual pathways of the goldfish: an immunohistochemical study. J Comp Neurol 285: 231–245.

46. Lillo C, Velasco A, Jimeno D, Lara JM, Aijon J (1998) Ultrastructural organization of the optic nerve of the tench (Cyprinidae, Teleostei). J Neurocytol 27: 593–604.
47. Downs JC, Roberts MD, Burgoyne CF (2008) Mechanical environment of the optic nerve head in glaucoma. Optom Vis Sci 85: 425–435.
48. Easter SS, Jr., Rusoff AC, Kish PE (1981) The growth and organization of the optic nerve and tract in juvenile and adult goldfish. J Neurosci 1: 793–811.
49. Maggs A, Scholes J (1986) Glial domains and nerve fiber patterns in the fish retinotectal pathway. J Neurosci 6: 424–438.
50. Sun D, Lye-Barthel M, Masland RH, Jakobs TC (2009) The morphology and spatial arrangement of astrocytes in the optic nerve head of the mouse. J Comp Neurol 516: 1–19.
51. Howell GR, Libby RT, Jakobs TC, Smith RS, Phalan FC, et al. (2007) Axons of retinal ganglion cells are insulted in the optic nerve early in DBA/2J glaucoma. J Cell Biol 179: 1523–1537.
52. Nickells RW (2007) From ocular hypertension to ganglion cell death: a theoretical sequence of events leading to glaucoma. Can J Ophthalmol 42: 278–287.
53. Quigley HA (2005) Glaucoma: macrocosm to microcosm the Friedenwald lecture. Invest Ophthalmol Vis Sci 46: 2662–2670.
54. Colavincenzo J, Levine RL (2000) Myelin debris clearance during Wallerian degeneration in the goldfish visual system. J Neurosci Res 59: 47–62.
55. Udvadia AJ (2008) 3.6 kb genomic sequence from Takifugu capable of promoting axon growth-associated gene expression in developing and regenerating zebrafish neurons. Gene Expr Patterns 8: 382–388.
56. Becker CG, Becker T (2007) Growth and pathfinding of regenerating axons in the optic projection of adult fish. J Neurosci Res 85: 2793–2799.
57. Hysi PG, Young TL, Mackey DA, Andrew T, Fernandez-Medarde A, et al. (2010) A genome-wide association study for myopia and refractive error identifies a susceptibility locus at 15q25. Nat Genet 42: 902–905.
58. Solouki AM, Verhoeven VJ, van Duijn CM, Verkerk AJ, Ikram MK, et al. (2010) A genome-wide association study identifies a susceptibility locus for refractive errors and myopia at 15q14. Nat Genet 42: 897–901.
59. Thorleifsson G, Walters GB, Hewitt AW, Masson G, Helgason A, et al. (2010) Common variants near CAV1 and CAV2 are associated with primary open-angle glaucoma. Nat Genet 42: 906–909.
60. Easter SS, Jr., Hitchcock PF (1986) The myopic eye of the Black Moor goldfish. Vision Res 26: 1831–1833.
61. Raymond PA, Hitchcock PF, Palopoli MF (1988) Neuronal cell proliferation and ocular enlargement in Black Moor goldfish. J Comp Neurol 276: 231–238.
62. Thanos S, Naskar R (2004) Correlation between retinal ganglion cell death and chronically developing inherited glaucoma in a new rat mutant. Exp Eye Res 79: 119–129.
63. Mii A, Nakajima T, Fujita Y, Iino Y, Kamimura K, et al. (2007) Genetic association of low-density lipoprotein receptor-related protein 2 (LRP2) with plasma lipid levels. J Atheroscler Thromb 14: 310–316.
64. Kamatani Y, Matsuda K, Okada Y, Kubo M, Hosono N, et al. (2010) Genome-wide association study of hematological and biochemical traits in a Japanese population. Nat Genet 42: 210–215.
65. Patel N, Hejkal T, Katz A, Margalit E (2007) Ocular manifestations of Donnai-Barrow syndrome. J Child Neurol 22: 462–464.
66. Rymer J, Wildsoet CF (2005) The role of the retinal pigment epithelium in eye growth regulation and myopia: a review. Vis Neurosci 22: 251–261.
67. Anzenberger U, Bit-Avragim N, Rohr S, Rudolph F, Dehmel B, et al. (2006) Elucidation of megalin/LRP2-dependent endocytic transport processes in the larval zebrafish pronephros. J Cell Sci 119: 2127–2137.
68. Carro E, Spuch C, Trejo JL, Antequera D, Torres-Aleman I (2005) Choroid plexus megalin is involved in neuroprotection by serum insulin-like growth factor I. J Neurosci 25: 10884–10893.
69. Christensen EI, Willnow TE (1999) Essential role of megalin in renal proximal tubule for vitamin homeostasis. J Am Soc Nephrol 10: 2224–2236.
70. Hammad SM, Ranganathan S, Loukinova E, Twal WO, Argraves WS (1997) Interaction of apolipoprotein J-amyloid beta-peptide complex with low density lipoprotein receptor-related protein-2/megalin. A mechanism to prevent pathological accumulation of amyloid beta-peptide. J Biol Chem 272: 18644–18649.
71. Zarbalis K, May SR, Shen Y, Ekker M, Rubenstein JL, et al. (2004) A focused and efficient genetic screening strategy in the mouse: identification of mutations that disrupt cortical development. PLoS Biol 2: e219. doi:10.1371/journal.pbio.0020219.
72. Dirnagl U, Simon RP, Hallenbeck JM (2003) Ischemic tolerance and endogenous neuroprotection. Trends Neurosci 26: 248–254.
73. Roth S (2004) Endogenous neuroprotection in the retina. Brain Res Bull 62: 461–466.
74. Hitchcock PF, Raymond PA (2004) The teleost retina as a model for developmental and regeneration biology. Zebrafish 1: 257–271.
75. John SW, Smith RS, Savinova OV, Hawes NL, Chang B, et al. (1998) Essential iris atrophy, pigment dispersion, and glaucoma in DBA/2J mice. Invest Ophthalmol Vis Sci 39: 951–962.
76. Anderson MG, Smith RS, Hawes NL, Zabaleta A, Chang B, et al. (2002) Mutations in genes encoding melanosomal proteins cause pigmentary glaucoma in DBA/2J mice. Nat Genet 30: 81–85.
77. Buckingham BP, Inman DM, Lambert W, Oglesby E, Calkins DJ, et al. (2008) Progressive ganglion cell degeneration precedes neuronal loss in a mouse model of glaucoma. J Neurosci 28: 2735–2744.
78. Soto I, Oglesby E, Buckingham BP, Son JL, Roberson ED, et al. (2008) Retinal ganglion cells downregulate gene expression and lose their axons within the optic nerve head in a mouse glaucoma model. J Neurosci 28: 548–561.
79. Murray M (1982) A quantitative study of regenerative sprouting by optic axons in goldfish. J Comp Neurol 209: 352–362.
80. Zhou LX, Wang ZR (2002) [Changes in number and distribution of retinal ganglion cells after optic nerve crush in zebrafish]. Shi Yan Sheng Wu Xue Bao 35: 159–162.
81. Berkelaar M, Clarke DB, Wang YC, Bray GM, Aguayo AJ (1994) Axotomy results in delayed death and apoptosis of retinal ganglion cells in adult rats. J Neurosci 14: 4368–4374.
82. Quigley HA (1985) Early detection of glaucomatous damage. II. Changes in the appearance of the optic disk. Surv Ophthalmol 30: 111, 117-126.
83. Villegas-Perez MP, Vidal-Sanz M, Bray GM, Aguayo AJ (1988) Influences of peripheral nerve grafts on the survival and regrowth of axotomized retinal ganglion cells in adult rats. J Neurosci 8: 265–280.
84. Murray M (1976) Regeneration of retinal axons into the goldfish optic tectum. J Comp Neurol 168: 175–195.
85. Sperry RW (1948) Patterning of central synapses in regeneration of the optic nerve in teleosts. Physiol Zool 21: 351–361.
86. Allcutt D, Berry M, Sievers J (1984) A qualitative comparison of the reactions of retinal ganglion cell axons to optic nerve crush in neonatal and adult mice. Brain Res 318: 231–240.
87. Liu X, Hawkes E, Ishimaru T, Tran T, Sretavan DW (2006) EphB3: an endogenous mediator of adult axonal plasticity and regrowth after CNS injury. J Neurosci 26: 3087–3101.
88. Spoelgen R, Hammes A, Anzenberger U, Zechner D, Andersen OM, et al. (2005) LRP2/megalin is required for patterning of the ventral telencephalon. Development 132: 405–414.
89. Willnow TE, Hilpert J, Armstrong SA, Rohlmann A, Hammer RE, et al. (1996) Defective forebrain development in mice lacking gp330/megalin. Proc Natl Acad Sci U S A 93: 8460–8464.
90. Westerfield M. EugeneOregon: The Zebrafish Book: University of Oregon Press,.
91. Charman WN, Tucker J (1973) The opitcal system of the goldfish eye. Vision Res 13: 1–8.